Nigerian Journal of Technology (NIJOTECH)
Vol. 41, No. 4 July, 2022, pp.712 –728
www.nijotech.com

Print ISSN: 0331-8443
Electronic ISSN: 2467-8821
http://dx.doi.org/10.4314/njt.v41i4.9

Mathematical and Simulation-Based Analysis of the Thermal and Electrical Performance of a Flat Plate Solar Air Heater Coupled with Thermoelectric Generators (TEGs)

A. C. Kalu-Uka[*,1], H. O. Njoku[2], C. A. Mgbemene[3]

[1,2,3]*Department of Mechanical Engineering, University of Nigeria, Nsukka, Enugu State, NIGERIA*

Article history: Received 22 May 2022; Revised form 12 August 2022; Accepted 12 August 2022; Available online 10 September 2022

Abstract

The thermal performance of a flat plate solar air heater coupled with thermoelectric generators has been studied. A model of the collector was designed and simulations using SCILAB software were carried out to assess its performance. The design was carried out by analyzing the various heat and mass transfer processes which occurred in the components of the air heating system. The analysis resulted in the formulation of mathematical expressions that modeled the conversion of solar energy from the sun into thermal energy absorbed by the air flowing through the collector. The temperatures of the various components of the collector were determined using the finite forward difference discretization method. The cumulative energy generated by the heat source was 87 MJ while the energy gained by the heated exit air amounted to 37 MJ, bringing about a system thermal efficiency of 42%. The electrical efficiency of the model was 8.3%.

Keywords: Renewable (solar) energy, heat and electricity generation, flat plate air heater, thermoelectric generator, efficiency

1.0 INTRODUCTION

The number of people living on the surface of the earth is on a steady increase with each turn of the year. The growth of world population together with rising material needs has escalated the rate of energy usage. Rapid increase in energy usage characteristic of the past 50-100 years cannot continue indefinitely as finite energy resources of the earth are exhaustible [1]. Simply put, the world is running out of energy from oil, coal, gas etc. to cater for the needs of the huge earth population. Meeting the ever-increasing demand of energy without degrading the environment has always been a concern of the scientific community [2]. There is therefore the need to explore the renewable energy sources to meet the energy demand in the present context [3]. Among all the renewable energy sources, solar energy has emerged as one of the most promising renewable energy resources, since it is abundant, freely available, and it has commercial potential too. It is widely known that solar energy is the one most abundant renewable energy source and emits energy at a rate of 3.8×10^{23} kW. Out of this amount, 1.8×10^{24} kW is absorbed by the earth [4]. This amount of energy is so vast that the entire world can comfortably tap into it and still have enough to spare. However, due to relative slowness in the creation and adoption of solar energy harnessing technologies, this energy source is still underutilized. Conversion of solar energy into thermal energy is the easiest and the most widely accepted method. This is done using absorbers of collectors. In most collectors, the designs are made with the view of generating more heat through the respective working fluids flowing over the absorbers when the absorbers trap incident radiation from the sun.

Research has shown that the heat energy from some of these collectors is large enough to be used for electricity generation [5-7]. These works demonstrate that there are real prospects in generating electricity for micro power applications from the heat energy absorbed in the collector. This is made possible through the principle of thermoelectricity, the direct conversion of temperature gradient to electrical potential difference.

A flat plate solar air collector primarily consists of a cover glass, an absorber plate, insulation, and space through which air flows. The cover glass protects the absorber from dust and scratches while trapping radiation

***Corresponding author **(Tel:** +234 (0) 8035600524**)**
Email addresses: *abraham.kalu-uka@unn.edu.ng* (A. C. Kalu-Uka), *howard.njoku@unn.edu.ng* (H. O. Njoku), *chigbo.mgbemene@unn.edu.ng* (C. A. Mgbemene)

from the sun within the collector. The absorber plate is the component that absorbs the radiation from the sun. It is made of a material that has high absorptivity. It is also important to reduce heat losses in the collector especially from the absorber plate, which is the component that transfers heat to the fluid medium flowing through the collector. Heat can be lost through conduction, radiation and convection. Some good thermal insulators which could be used in collectors are the glass wool with a low thermal conductivity of 0.045W/mK, polyurethane rigid foam (0.0245W/mK), foam rubber (0.05 W/mK) etc. [8].

The absorber (heat exchanger) may have embedded or bonded tubes for heat exchange to water or air. It may also have plates, fins or be a porous mat for heat exchange to air. On exposure to sun's radiation, absorbers of flat plate collector get heated up to temperatures between 70ºC to 90ºC [9]. Although this temperature range appears to be low, specially designed thermoelectric systems have no difficulty generating useful electricity (for low power applications) within this temperature range. All that is needed is to couple TEGs to the hot side of the absorber (heat source) and allow for a cold side (heat sink) to provide for a temperature difference. In this setting, the TEGs would utilize the difference in the temperatures between the two dissimilar materials of the heat source and heat sink to generate electricity. Thus, the use of TEGs provides quite several opportunities for electric power generation as they have been specially designed to operate with even very small heat sources. Research by Snyder has shown that they can be miniaturized to even harvest the heat from the human body, in order to power wearable gadgets like wristwatch [10].

There have been previous studies on generation of heat from solar air collectors and thermoelectric generators. Neville [11] proposed that instead of making use of pipes as the channel through which air is circulated to absorb heat and transport it to the point of use, one can conveniently use a metal sheet. In this way fluid can flow over unrestricted on the heated metal sheet. This idea supports the use of sheet flat plate air collectors to effectively collect heat instead of the traditional scenario where flat plate collectors use tubes or cans for heat collection. This method reduces the complexities involved in using tubes as absorber surfaces. Enibe [12], stated that the airflow rate through the absorber plate is determined by balancing the buoyancy head resulting from thermally induced density differences and the friction head due to viscous flow resistances. The balancing of buoyancy head was done by taking the pressure change in the horizontal direction to be negligible. Saxena et al [13] conducted a thermodynamic review of solar air heaters. They pointed out that allowing a flow of the air above the absorber increases the convection losses from the glazing. To decrease these losses, they advised that selective coating should be applied to improve the solar air heater efficiency. Eze and Ojike [14] worked on a passive solar water heater and observed that the peak temperature rise of the heated water was about 83ºC, while the maximum daily average useful efficiency was about 42%. They concluded that the system can be operated successfully for agro-industries and home applications. Indrajit et al [15] reported the results of experimental studies on two non-porous solar absorber air heaters with and without fins and found that air heaters with fins are more efficient in comparison to the air heater without fins for air flow rates ≤ 0.0388kg/s. Singh and Bansal [16] fabricated a solar air heater using broken glass pieces as absorber surface. He reported that the efficiency of the collector continues to increase as air mass flow rate increased. Thermoelectricity is the direct conversion of temperature gradient to electrical potential difference primarily through the Seebeck effect. Devices that used the principle of thermoelectricity are called Thermoelectric Generators, TEGS. Bjork et al [17], argued for the performance of a TEG to be estimated using numerical modeling before actual physical modules are constructed. This allows for the development of new and better thermoelectric generators in a cost-effective manner, as well as for designing and optimizing modules to achieve the highest possible efficiency. Mgbemene et al [6] explored the concept of a compound parabolic concentrator with a thermoelectric module to produce electricity from the sun. The work mathematically modeled the system with the development of equations of heat and electric power transfer within the system. A simple prototype was built and the measurements and tests that were conducted were appropriately in line with the model predictions and established the proof-of-concept. Biswas et al [18] stated that the typical efficiency of TEGS was around 5-8%. Older devices used bimetallic junctions and were bulky. More recent devices use highly doped semiconductors made from Bismuth Telluride Bi_2Te_3, Lead Telluride Pb_2Te_3, Calcium Manganese Oxide CaMnO, or combinations thereof, depending on the temperature. Snyder [10] presented a one-dimensional model of a TEG where there were no heat losses and recorded an efficiency of 9%. Rowe [19] reported that thermal efficiency is an important parameter and provides valuable information for designing systems. The TEG used in the work is a model TEC1-12706 Bismuth Telluride device with a physical size of (40×40×3.5) mm. The device has 127 couples. In the experiment, the load resistance was 0.488 Ohms, and the applied voltage was varied from 12, 14, 16, 18, 20 and 22

volts. The lowest temperature difference tested was 20.6ºC corresponding to a heater voltage of 12 Volts and the highest temperature difference tested was 68.1ºC corresponding to a heater voltage of 22 Volts. The highest temperature difference produced the highest power output. The efficiency of the device throughout the test was determined. The efficiency increases with increasing change in temperature and with the highest temperature change evaluated at 68.1ºC, the maximum efficiency was 2.22%. The maximum power generated with this singular TEG, at 68.1ºC, was 1.17 Watts. Amatya et al [7] showed that running a solar thermoelectric generator using cheap concentrators with high Figure of Merit, ZT, modules can be a cost-effective alternative to solar photovoltaics for micro-power generation.

They presented a thermodynamic analysis for predicting the thermal-to-electrical conversion efficiency for the generator. They found out that with novel thermoelectric materials which had high material ZT, a system efficiency of 5.6% can be achieved. However experimentally they got an efficiency of 3% with a commercial Bismuth Telluride, Bi2Te3, module, which to the best of their knowledge at the time of research, was the highest efficiency for solar thermoelectric using a module.

From the works already listed, it can be inferred that heat and electricity can be individually generated from solar energy using solar collectors. However, what has not been done (to the best of the knowledge of the authors) is combining the simultaneous generation of heat and electricity from one flat plate collector system. This coupling is a novelle idea as it saves time and both financial and material resources in the production of one collector that serves two purposes. This gives rise to the motivation of this research, which is to study the feasibility of generating both heat and electricity through the coupling of flat plate air heater with Thermoelectric Generators, TEGs.

2.0 METHODOLOGY

In Fig. 1, I_T is the insolation from the sun, Q_{loss} is the heat loss from the glass to the sky by convection and radiation, Q_h is the rate of heat energy absorbed in the absorber plate (heat source of thermoelectric generators, TEGs), Q_c is the rate of heat energy dissipated at the heat sink of the TEGs, T_{int} is the effective temperature of the air at the opening between the two absorber plate segments, T_{exit} is the effective temperature of the heated air leaving the collector, θ is the tilt angle of the collector, *L1* and *L2* are the lengths of the first and second glass segments respectively, $\dot{m}_{in}$ and $\dot{m}_{out}$ are the inlet and outlet air mass flow rates flowing through the collector.

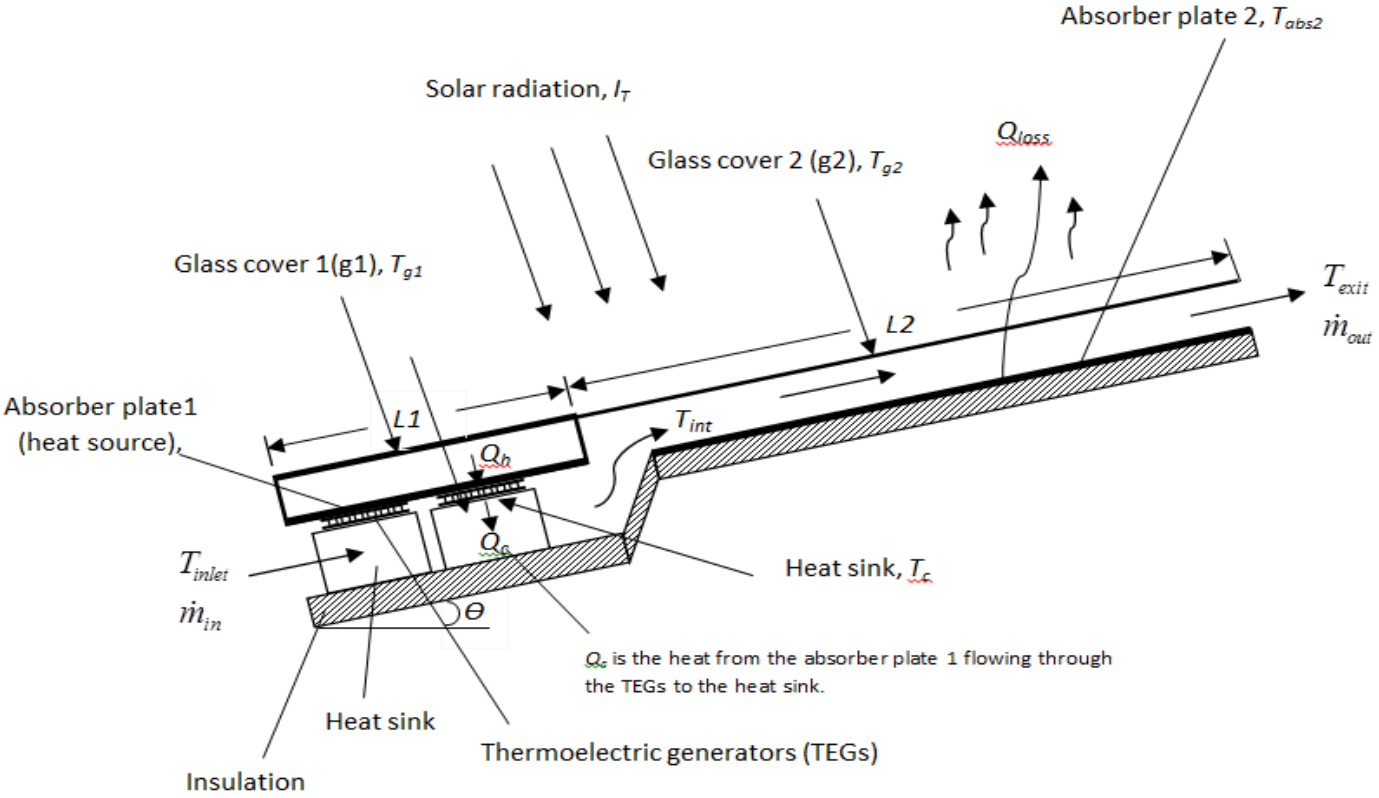

Figure 1: A Schematic diagram of the solar collector.

2.1 Configuaration(Diagram) of the system

The diagram presented in Fig. 1 is the schematic diagram of the solar collector.

2.1.1 Assumptions made for the collector system

Thefollowing assumptions are made for the collector system

1. The system is in transient state
2. There is no heat generation within the system
3. The air has constant density
4. There is no shaft work in the fluid
5. One dimensional flow in x-direction, $V_y = 0$.
6. Viscosity of the air is negligible
7. Negligible friction heating

2.1.2 Physical description of the flat plate air heater collector-TEG system

The Flat Plate (Solar Air Heater) collector design as shown in Fig. 1, is made up of a single glass cover, two absorber plate segments which are coated with selective surfaces having high absorptivity for radiant energy, a bank of thermoelectric generators, (TEGs) connected in a combined series (electrically) and parallel (thermally) arrangement and a channel of rectangular cross-section for the inlet air.

2.1.3 Operating principle of the conjugate TEG flat plate air collector

After the solar collector has been exposed to irradiation, and as the radiant energy from the sun heats up the second segment of the absorber surface, the air just above the second absorber segment gets heated up. Through the principle of bouyancy of forces, this mass of heated air rises along the inclined surface of the solar collector to get to the exit, thus creating a pressure difference that can only be balanced when a denser fluid, in this case a mass of air (of lower temperature) takes its original space. This cold mass of air is supplied (as a results of the bouyancy forces generated because of density differences between two fluids at different temperatures [6]), through a rectangular inlet at a rate, $\dot{m}_{in}$. As the cold air enters the collector, it, first of all, cools the cold side of the TEG banks and gets slightly heated up in the process. It then flows through opening between the absorber plate segments. On entering the space above the second absorber plate segment, it continues to rise along the absorber plate because of its decreasing density, at a rate, $\dot{m}_{out}$, to the exit.

After considerable heating at the surface of the absorber plate by the radiation from the sun, and by extension the top surfaces (hot side) of the TEGs (which were integrated into the absorber plate), a uniform hot temperature is reached, T_h. At the bottom of the TEGs is the heat sink. This space comprises the area where the cold mass of air enters the collector through the rectangular pipe at the rate, $\dot{m}_{in}$ and first cools the lower side of the TEGs.

2.2 Mass balance in the flat plate collector

The difference between the mass flow rate of the air flowing into the collector, $\dot{m}_{in}$ and the mass flow rate of the air exiting the collector, $\dot{m}_{out}$ is equal to the rate of air accumulation, $\frac{dm_{col}}{dt}$, in the space between the absorber plate and the cover glass.

Mathematically,

$$\dot{m}_{in} - \dot{m}_{out} = \frac{dm_{col}}{dt} \tag{2.1}$$

Assuming a steady state condition, there is no accumulation of air in the system.

$$\frac{dm_{col}}{dt} = 0 \tag{2.2}$$

$$\therefore \dot{m}_{in} = \dot{m}_{out} \tag{2.3}$$

The above equation implies that the air mass flow rate, $\dot{m}$ is the same at any channel cross section.

2.3 Energy analysis of the flat plate collector

The energy analysis of the solar collector is carried out taking one component at a time and analysing each one separately.

2.4 Heat transfer in the cover glass segments

The net rate of energy accumulation in the glazing is equal to the difference between the rate of energy striking the surface of the cover glass and the rate of energy leaving the surface. For purposes of clarity, the cover glass is defined by two equations which describe the heat flows in segments 1 and 2 of the glass cover.

The energy equation for the glass cover of the first segment, g_1 is given as follows:

$$\begin{aligned} m_{g1}c_{p_g}\frac{dT_{g1}}{dt} = {} & \alpha_g A_{g1} I_T - h_{c,g1-amb}A_{g1}\left(T_{g1} - T_{amb}\right) \\ & - h_{r,g1-sky}A_{g1}\left(T_{g1} - T_{sky}\right) \\ & + h_{r,abs1-g1}A_{g1}\left(T_{abs1} - T_{g1}\right) \\ & + h_{c,abs1-g1}A_{g1}\left(T_{abs1} - T_{g1}\right) \end{aligned} \tag{2.4}$$

The energy equation for the glass cover of the second segment, g_2 is given as follows:

$$m_{g2}c_{p_g}\frac{dT_{g2}}{dt} = \alpha_g A_{g2} I_T - h_{c,g2-amb}A_{g2}(T_{g2}-T_{amb}) - h_{r,g2-sky}A_{g2}(T_{g2}-T_{sky}) + h_{c,air2-g2}A_{g2}(T_{air2}-T_{g2}) + h_{r,abs2-g2}A_{g2}(T_{abs2}-T_{g2}) \quad (2.5)$$

where $m_{g\,1}$, m_{g2} = the masses of the glass segments 1 and 2 (kg)

c_{pg} = the specific heat capacity of the glass (J/kg.K)

α_g = the absorptivity of the glass

$A_{g,1}$, $A_{g,2}$ = the surface areas of the glass segments 1 and 2 (m^2)

I_T = the prevailing solar radiation intensity (W/m^2)

$h_{c,g\text{-}amb}$ = the convection heat transfer coefficient from the glass to the ambient (W/m^2K)

$h_{r,g\text{-}sky}$ = the radiation heat transfer coefficient from the glass to the sky (W/m^2K)

$h_{r,abs\text{-}g}$ = the radiation heat transfer coefficient from the absorber to the glass (W/m^2K)

$h_{c,air\text{-}g}$ = the convection heat transfer coefficient from the air to the glass (W/m^2K)

$T_{g,1}$, $T_{g,2}$, $T_{amb,}$,T_{abs1},T_{abs1},T_{air2},T_{sky} = the temperatures of the glass segments 1 and 2, the ambient air above the glass, the absorber segments 1 and 2, the air flowing over the absorber segment 2, and the sky, respectively.

The radiation heat transfer coefficient from the glass to the ambient is given by [20]

$$h_{r,g-sky} = \frac{\sigma\varepsilon_g(T_g^{\,2}+T_{sky}^{\,2})(T_g+T_{sky})(T_g-T_{sky})}{T_g-T_{amb}} \quad (2.6a)$$

where the sky temperature, T_s (K), is given by [21]

$$T_s = 0.0553\left(T_a^{\,1.5}\right) \quad (2.6b)$$

and T_a (K) is the temperature of the ambient.

The radiation heat transfer coefficient from the absorber to the glass is given by [22]

$$h_{r,abs-g} = \frac{\sigma(T_{abs}^{\,2}+T_g^{\,2})(T_{abs}+T_g)}{\frac{1-\varepsilon_{abs}}{\varepsilon_{abs}}+\frac{1}{F_{abs,g}}+\frac{(1-\varepsilon_g)A_{abs}}{\varepsilon_g A_g}} \quad (2.7a)$$

where σ is the Stephan Boltzmann constant and ε_{abs}, ε_g are the characteristic emissivities of the absorber surfaces and the glass respectively and $F_{abs,g}$ is the view factor of radiation from the absorber surface to the glass.

A further simplification to equation 2.7a can be written as $F_{abs,g} = 1$ and $A_{abs} = A_g$. Thus

$$h_{r,abs-g} = \frac{\sigma(T_{abs}^{\,2}+T_g^{\,2})(T_{abs}+T_g)}{\frac{1-\varepsilon_{abs}}{\varepsilon_{abs}}+\frac{1-\varepsilon_g}{\varepsilon_g}} \quad (2.7b)$$

Free or natural convection heat transfer data are usually correlated in terms of two or three dimensionless parameters: the Nusselt number, *Nu*, the Raleigh number, *Ra*, and the Prandtl number, *Pr*, with the Nusselt, Rayleigh and Prandtl numbers expressed in [8] as

$$Nu = \frac{hL}{k} \quad (2.8a)$$

$$Ra = \frac{g\beta\Delta TL^3}{\nu^2} \quad (2.8b)$$

$$\Pr = \frac{\nu}{\alpha} \quad (2.8c)$$

where

h = convective heat transfer coefficient [W/m^2K]

L = plate spacing [m]

k = thermal conductivity of the air between the glass and the absorber plate [W/mK]

g = gravitational constant [m/s^2]

β = volumetric coefficient of expansion of the air (for an ideal gas, $\beta = 1/T$)[1/K]

ΔT = temperature difference between the absorber plate and the glass [K]

ν = kinematic diffusivity of the air [m^2/s]

α = thermal diffusivity of the air [m^2/s]

The coefficient of convective heat transfer between the absorber plate and the glass, $h_{c,abs1\text{-}g1}$ may be obtained using the Hollands et al [8] relationship which relates the Nusselt number and Rayleigh number for tilt angles, θ, from 0 to 75^0. It is expressed as

$$Nu = 1 + 1.44\left[1 - \frac{1708(sin1.8\theta)^{1.6}}{Racos\theta}\right]\left[1 - \frac{1708}{Racos\theta}\right]^{+} + \left[\left(\frac{Racos\theta}{5830}\right)^{1/3} - 1\right]^{+} \quad (2.9)$$

where the + superscript implies that only positive values of the terms in the square brackets are to be used (i.e. use zero if the term is negative).

The convection heat transfer coefficients from the glass to the ambient, $h_{c,g1\text{-}amb}$ can be obtained using the McAdams correlation and is expressed in [8] as

$$h = 5.7 + 3.8V \quad (2.10)$$

where V is the wind speed in m/s.

2.5 *Heat transfer mechanism in the mass of air passing through the collector within the second absorber segment*

The rate of energy gain in the air passing over the second absorber segment with a mass flow rate, is equal to the sum of the rate of heat energy absorbed by the air from the second absorber segment, the rate of heat energy from the glass to the air and the rate of energy gain by the air flowing between the exit and inlet points of the second absorber segment. This is expressed as

$$m_{air}c_{p,air}\frac{dT_{air2}}{dt} = h_{c,abs2-air2}A_{abs2}(T_{abs2} - T_{air2}) + h_{c,air2-g2}A_{abs2}(T_{g2} - T_{g2}) + mc_{p,air}(T_{int} - T_{exit}) \quad (2.11a)$$

where T_{int} and T_{exit} are the effective temperatures of the air at the opening between the two absorber plate segments and at the exit of the collector respectively, A_{abs2} is the area of the second absorber segment, m_{air} is the mass of air flowing through the collector and cp_{air} is the specific heat capacity of the air.

Assuming that T_{exit} is the same as T_{air2} and T_{int} is the same as T_{air1}, equation 2.11a is expressed as

$$m_{air}c_{p,air}\frac{dT_{air2}}{dt} = h_{c,abs2-air2}A_{abs2}(T_{abs2} - T_{air2}) + h_{c,air2-g2}A_{abs2}(T_{g2} - T_{g2}) + mc_{p,air}(T_{air} - T_{air2}) \quad (2.11b)$$

The convection heat transfer coefficient from the second absorber plate to the air flowing over it $h_{c,abs2\text{-}air2}$, can be obtained from Cengel and Ghajar, [23] using the expressions below:

$$Nu = 0.54Ra_L^{1/4} \quad (2.12a)$$

$$Ra = \frac{g\beta(T_{abs2} - T_{air2})L^3}{\nu^2}\Pr \quad (2.12b)$$

$$h_{c,abs2-air2} = \frac{k}{L}Nu \quad (2.12c)$$

where L is the characteristic length and is given by:

$$L = \frac{A}{P} \quad (2.12d)$$

and A and P are the area and perimeter of the surface of the second absorber segment respectively.

The convection heat transfer coefficient for the air flowing across the second absorber segment to the second glass segment, $h_{c,air2\text{-}g2}$, can be obtained from the expressions in [23] below:

$$Nu = 0.15Ra_L^{1/3} \quad (2.13a)$$

$$Ra = \frac{g\beta(T_{g2} - T_{air2})L^3}{\nu^2}\Pr \quad (2.13b)$$

$$h_{c,air2-g2} = \frac{k}{L}Nu \quad (2.13c)$$

The rate of change in the energy of the air passing through the inlet of the collector is the net sum of the rate of heat energy absorbed by this air (as a result of convection both from the heat sink surface without fins and the finned surfaces) as it flows from the inlet through the heat sink to the intermediate point, to become T_{int} (T_{air1}), and from where it would flow into the second absorber plate.

$$m_{air}c_{p,air}\frac{dT_{air1}}{dt} = mc_{p,air}(T_{amb} - T_{air1}) + Q_c - U_{loss}A_{insul}(T_{air1} - T_{amb}) \quad (2.14)$$

where the inlet temperature to the heat sink is the ambient temperature, T_{amb}, T_{air1} is the temperature of the inlet air that has picked up energy from the heat sink, Q_c is the heat dissipated at the heat sink and A_{insu1} is the surface area of the layer of insulation used to pad the bottom of the enclosure housing the heat sink and is assumed to be equal to the area of the first absorber segment, A_{abs1}. $U_{loss,}$ is the

heat loss coefficient through the insulator and is expressed as

$$U_{loss} = \frac{K_{insu} h_{insu}}{L_{insu} h_{insu} + K_{insu}} \quad (2.14b)$$

where K_{insu} is the thermal conductivity of the insulation, h_{insu} is the convection heat transfer coefficient from the insulation to the ambient and L_{insu} is the thickness of the insulation. Equation 2.14b is derived from equating two different formula used for calculating heat flow rate, $\dot{Q}$.

The first heat flow rate is expressed in terms of the insulation surface area, A_{insu1}, overall heat transfer coefficient of the insulation, U_{loss}, and the temperature difference, ΔT, between the air on one side of the insulation and the ambient. Thus

$$\dot{Q} = A_{insu1} U_{loss} \Delta T \quad (2.14c)$$

The other heat flow rate is expressed in terms of the temperature difference, ΔT, between the air on one side of the insulation and the ambient and the effective thermal resistance of both the insulation and the ambient, R_{th}. Thus

$$\dot{Q} = \frac{\Delta T}{R_{th}} \quad (2.14d)$$

R_{th} is the effective resistance from the resistances offered by the series arrangement of the insulation, $(L_{insu}/K_{insu}A_{insu1})$, and the ambient, $(1/A_{insu1}h_{insu})$.

2.6 Heat transfer in the absorber plates

For the first absorber plate segment, the rate of change of energy in the absorber plate is equal to the net sum of all rates of energy absorbed in the absorber plate as well as lost from the plate. Mathematically it can be expressed as:

$$m_{abslr} c_{pabs} \frac{dT_{abs1}}{dt} = \tau_g \alpha_{abs1} A_{abs1} I_T - h_{r,abs1-g1} A_{abs1} (T_{abs1} - T_g) - h_{c,abs1-g1} A_{abs1} (T_{abs1} - T_{g1}) - Q_h \quad (2.15)$$

where τ_g is the transmisivity of the glass, α_{abs} is the absorptivity of the glass segment, Cp_{abs} is the specific heat capacity of the absorber, $h_{r,abs1-g1}$ and $h_{c,abs1-g1}$ can be obtained from equations 2.7b and equations 2.8a, 2.8b, 2.8c, 2.9 respectively. Q_h is the effective heat conduction into the top surfaces of the hot sides of the TEGs.

The rate of change of energy in the second absorber plate is the difference between all the energy absorbed by the absorber plate and the energy lost from the absorber plate. It is given by

$$m_{abslr} c_{pabs} \frac{dT_{abs2}}{dt} = \tau_g \alpha_{abs1} A_{abs2} I_T - h_{r,abs2-g2} A_{abs,2} (T_{abs2} - T_{g2}) - h_{c,abs2-air2} A_{abs1} (T_{abs2} - T_{air2}) - U_{loss} + A_{insu2} (T_{abs2} - T_{air2}) \quad (2.16)$$

where $h_{r,abs2-g2}$ is given by equation 2.7, $h_{c,abs2-air2}$ is given by equations 2.12a, 2.12b and 2.12c, T_{air2} is the temperature of the air flowing over the second absorber segment, and U_{loss} is the heat loss coefficient through the insulator beneath the second absorber segment. It can be expressed using equation 2.14b.

2.7 Thermal and electrical analysis of the TEG element

A sketch of the TEG is shown in Fig. 2.

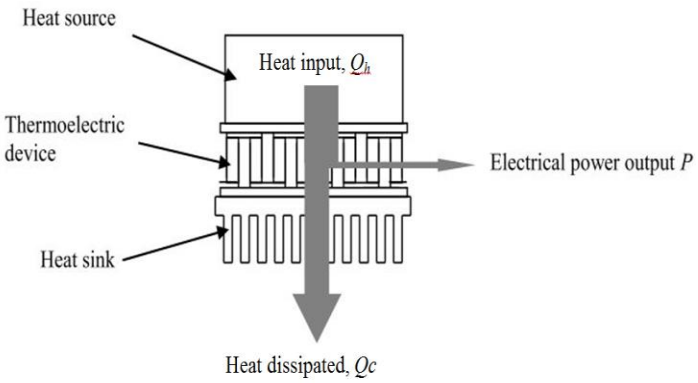

Figure 2: A labeled diagram of the solar collector [6]

The rate of heat flow into the hot side, Q_h, is the net sum of the rate of heat energy absorbed at the top surface of the TEGs by the Peltier Effect, $\alpha I T_h$, and by conduction from the absorber plate to the top surface of the TEGs, $K\Delta T$, and the heat lost by resistive heating of the TEGs as the heat flows down through the thermoelectric elements to the heat sink, I^2R. Q_h is expressed as:

$$Q_h = N\alpha I T_h + K\Delta T - 0.5 I^2 R \quad (2.17)$$

Where N is the number of thermoelectric elements in each thermoelectric generator, α is the seebeck coefficient, I is the current generated, T_h is the effective temperature at the hot side of the TEGs and is assumed to be equivalent to the temperature of the absorber plate 1, ΔT is the temperature difference between the temperatures at the hot side of the TEGs, T_h, and the cold side heat sink, T_c, i.e. $(T_h - T_c)$. K is the effective thermal conductance of the thermoelectric module expressed as:

$$K = 2N\frac{A_{th}k}{L_{th}} \tag{2.18a}$$

where k is the thermal conductivity of the thermoelements of the TEG, A_{th} is the surface area of each TEG and L_{th} is the length of the leg of a TEG thermoelement.
In equation 2.17, R is the effective internal resistance of the TEGs to the flow of current and is expressed as:

$$K = 2N\frac{\rho A_{th}}{L_{th}} \tag{2.18b}$$

where ρ is the resistivity of the thermoelements of the TEG. I in equation 2.17 is the electric current output from the TEGs is expressed as:

$$I = \frac{N\alpha(T_h - T_c)}{R + R_L} \tag{2.18c}$$

where the term, $\alpha(T_h\text{-}T_c)$ represents the open circuit voltage and R_L is the load resistance.

With T_h already approximated to be equal to T_{abs1} and the base of the heat sink temperature, T_c, still unknown. T_c can be deduced from the energy equation of the heat sink, taking into consideration the total number of fins attached to the heat sink and assuming that the heat dissipated at the heat sink is lost by convection through the surface of the fins to the inlet air flowing into the heat sink enclosure. Thus:

$$Q_c = n_f \eta_{fin} h_{fin} P_{fin} L_{fin}(T_c - T_{air1}) \tag{2.19}$$

where n_f is the number of fins, η_{fin} is the fin efficiency, h_{fin} is the convection heat transfer coefficient from the fin to the inlet air, P_{fin} is the perimeter of each fin base and L_{fin} is the vertical height of each fin.

The heat flow at the cold side of the TEGs, Q_c, is the net sum of the rate of heat energy dissipated at the heat sink of the TEGs by Seebeck Effect, by conduction from the absorber plate to the heat sink of the TEGs and by the heat gained by resistive heating of the TEGs as the heat flows down to the heat sink. Q_c is also expressed as:

$$Q_c = N\alpha I T_c + K\Delta T + 0.5I^2R \tag{2.20}$$

The electrical power output from the TEGs, P, is the difference between the rate of heat energy added to the top surface of the TEGs, Q_h, and the rate of heat energy dissipated in the heat sink, Q_c. It is expressed as:

$$P = n(N\alpha I(T_h - T_c) - I^2R) \tag{2.21}$$

where n is the number of TEGs used for the model.
The output voltage, V, is obtained by dividing the electrical power by the current output and is expressed as:

$$V = n(N\alpha(T_h - T_c) - IR) \tag{2.22}$$

The electrical efficiency of the thermoelectric generators is obtained from the ratio of the cumulative electrical power output, P_{cum}, to the cumulative thermal power input, $Q_{h,cum}$ into the TEGs and is expressed as

$$\eta_{elect} = \frac{P_{cum}}{Q_{h\,cum}} \tag{2.23a}$$

Where

$$Q_{h\ cum} = \tau_g \alpha_{abs} A_{abs1} I_T \tag{2.23b}$$

The area of the first absorber segment is used in equation 2.23b because the TEGs are coupled to the first absorber segment.

The cumulative energy gained by the air as it flows through the collector to the exit, E_{gain}, is the product of the air mass flow rate through the collector, the specific heat capacity of air and the temperature difference between the air temperature at the exit and at the inlet of the collector.

$$E_{gain} = \dot{m}c_{p\,air}(T_{air\,2} - T_{air\,1}) \tag{2.24a}$$

The cumulative energy absorbed by the collector, E_{abs}, is the product of the cumulative insolation received from the sun over the whole day, the transmitivity of the glass, the absorptivity of the absorber plate and the sum of the areas of both the first and second absorber segments. It is expressed as:

$$E_{abs} = \tau_g \alpha_{abs}(A_{abs1} + A_{abs2}) I_T \tag{2.24b}$$

The areas of both the first and second absorber segments are used in equation 2.24b because the air that flows through the collector and gains energy, first flows through the space beneath the first absorber segment to gain energy lost by the first absorber segment. Then it moves on to flow over the area of surface of the second absorber segment to the exit.

The overall efficiency of the flat plate air heating system coupled with the TEGs is given by the ratio of the cumulative energy gained by the heated exit air to the cumulative energy absorbed by the collector from the sun's radiation. It is expressed as:

$$\eta_{therm} = \frac{E_{gain}}{E_{abs}} \tag{2.24c}$$

2.8 Finite forward difference discretization expressions

Applying the Finite Forward Difference (FFD) discretization to equation 2.4, the temperature of the first glass segment at any time, T^1_{g1}, is expressed in terms of its previous temperature, T^o_{g1}, as:

$$\begin{aligned} T^1g1 = T^0g1 + \frac{\Delta t}{mg_1C_{pg}}(&\alpha_g A_{g1} I_T - h_{c,g1-amb}A_{g1}(T^0g1 - T^0{}_{amb}) \\ &- h_{r,g1-sky}A_{g1}\left(T^0_{g1} - T^0_{sky}\right) \\ &+ h_{r,abs1-g}A_{g1}\left(T^0_{abs1} - T^0_{g1}\right) \\ &+ h_{c,abs1-g1}A_{g1}((T^0abs1 - T^0{}_{g1}) \end{aligned} \tag{2.25a}$$

substituting $m_{g1} = \rho_g A_{g1} L_{g1}$ where ρ_g is the density of the glass and L_g is the thickness of the glass. Equation 2.25a can be further simplified and expressed as

$$\begin{aligned} T^1g1 = T^0g1 + \frac{\Delta t}{\rho_g C_{pg} L_g}(&\alpha_g I_T - h_{c,g1-amb}(T^0g1 - T^0{}_{amb}) \\ &- h_{r,g1-sky}\left(T^0_{g1} - T^0_{sky}\right) + h_{r,abs1-g}\left(T^0_{abs1} - T^0_{g1}\right) \\ &+ h_{c,abs1-g1}((T^0abs1 - T^0{}_{g1}) \end{aligned} \tag{2.25b}$$

Applying the FFD discretization to equation 2.5, the temperature of the second glass segment at any time, T^1_{g2}, is expressed in terms of its previous temperature, T^o_{g2}, as:

$$\begin{aligned} T^1g2 = T^0g2 + \frac{\Delta t}{\rho_g C_{pg} L_g}(&\alpha_g I_T - h_{c,g2-amb}(T^0g2 - T^0{}_{amb}) \\ &- h_{r,g2-sky}\left(T^0_{g2} - T^0_{sky}\right) + h_{C,air2-g2}\left(T^0_{air2} - T^0_{g2}\right) \\ &+ h_{r,abs2-g2}\left(T^0abs1 - T^0{}_{g2}\right) \end{aligned} \tag{2.26}$$

Applying the FFD discretization to equations 2.11b and 2.14, the temperatures of the air flowing over the second absorber plate and through the heat sink at any time T^1_{air2} and T^1_{air1}, respectively, are expressed in terms of their previous temperatures, T^o_{air2} and T^o_{air1} as:

$$\begin{aligned} T^1_{air,2} = T^0_{air,2} + \frac{\Delta t}{m_{air2}C_{pg}}(&h_{c,abs2-air2,}A_{abs}(T^0abs2 - T^0{}_{air2}) \\ &- h_{c,air2-g2}A_{abs2}\left(T^0_{air2} - T^0_{g2}\right) \\ &+ mc_{p\,air-g2}\left(T^0_{air1} - T^0_{air2}\right) \end{aligned} \tag{2.27}$$

$$\begin{aligned} T^1_{air,1} = T^0_{air,1} + \frac{\Delta t}{\rho_{air}C_{pair}L_{air\,gap}}\Bigg(&\left(\frac{1}{A_{abs1}}\right)mc_{p\,air}T_{amb} - T^0_{air,1} \\ &+ \left(\frac{1}{A_{abs1}}\right)Q_c \\ &- \left(\frac{1}{A_{abs1}}\right)U_{loss}A_{insull}\left(T^0_{air1} - T_{amb}\right)\Bigg) \end{aligned} \tag{2.28}$$

Applying the FFD discretization to equations 2.15 and 2.16, the temperatures of the first and second absorber plate segments in any given time, T^1_{abs1} and T^1_{abs2}, respectively are expressed in terms of their previous temperatures, T^o_{abs1} and T^o_{abs1} as:

$$\begin{aligned} T^1_{abs,1} = T^0_{abs1} + \frac{\Delta t}{\rho_{abs}C_{pabs}L_{abs}}\Big(&\tau_g\alpha_{abs}I_T - h_{r,abs-g1}\left(T^0_{abs1} - T^0_{g1}\right) \\ &- h_{c,abs1-g1}\left(T^0_{abs1} - T^0_{g1}\right) \\ &- h_{c,abs1-g1}\left(T^0_{abs1} - T^0_{g1}\right) - \frac{Q_h}{A_{abs1}}\Big) \end{aligned} \tag{2.29}$$

$$\begin{aligned} T^1_{abs,1} = T^0_{abs1} + \frac{\Delta t}{\rho_{abs}C_{pabs}L_{abs}}\Big(&\tau_g\alpha_{abs}I_T - h_{r,abs-g2}\left(T^0_{abs1} - T^0_{g2}\right) \\ &- h_{c,abs2-air2}\left(T^0_{abs1} - T^0_{air2}\right) \\ &- h_{c,abs2-air2}\left(T^0_{abs2} - T^0_{air2}\right) \\ &- U_{loss}\left(T^0_{abs2} - T^0_{amb}\right)\Big) \end{aligned} \tag{2.30}$$

Applying the FFD discretization to equation 2.19, the temperature of the base of the heat sink at any given time, T^1_c, as:

$$T^1{}_c = T^0{}_{air1} + \frac{Q_c}{n_f\eta_{fin}h_{fin}P_{fin}L_{fin}} \tag{2.31}$$

With equations (2.25b), (2.26), (2.27), (2.28), (2.29), (2.30), and (2.31), the temperatures of the various components of the conjugate flat plate collector and thermoelectric generators can be determined. These temperature values will be useful in determining other unknowns like the heat gained by the air flowing through the collector, the thermal efficiency of the collector, the

rate of heat absorption in the heat sink, the rate of heat dissipation in the heat source, the maximum power, voltage and current of the TEGs, and then the electrical efficiency of the TEGs coupled to the collector.

2.9 Numerical simulation

The finite forward equations for each section of the Solar Collector-TEG system (Equations: 2.25b, 2.26, 2.27, 2.28, 2.29, 2.30 and 2.31) were solved using SCILAB software to determine the various temperature profiles and the energy absorbed or dissipated as the case may be, using a time step of 0.1 second i.e. $\Delta t = 0.1s$. In developing the SCILAB codes (attached as additional file to this paper) for the program, representative atmospheric conditions were imposed on the governing equations of the flat plate air heater system and each simulation was allowed to run for one day.

2.10 Design parameters

The summary of the design parameters is presented in Tables 2.1, 2.2, 2.3, 2.4, 2.5, 2.6 and 2.7 in appendix. The properties of air, glass, absorber segments and insulation were gotten from Duffie and Beckmann, [8]. The characteristic properties of the TEG were mainly gotten from Angrist [24] and others were from Rowe [19]. Other parameters of the collector are due to the design objectives.

3.0 RESULTS AND DISCUSSION

3.1 Insolation and ambient temperature profiles

The models for insolation and ambient temperature used in the simulation process were adapted from Torchia-Nunez et al [25]. The resulting insolation values and ambient temperatures are shown in Fig. 3. From Fig. 3, it can be observed that insolation is zero prior to 6am, i.e. during the early hours of the day. But then the insolation gradually rises to its peak value (of 1000W/m^2) by midday. The ambient temperature experiences a corresponding rise and reaches its peak of 308K at about 2 hours after midday. From then on, both the insolation and the ambient temperature decrease as the day progresses.

3.2 Temperature distributions of the various components of the system

The various components of the system were assumed to be initially at a temperature of 298K, before the commencement of the simulation process. Simulations were performed using a maximum insolation of 1000W/m^2 for the 24 hours of a day and the graphs of temperatures of the different components of the solar collector are presented and discussed in the following sections. Only the daylight hours, starting from 6am to 6pm, are represented in the graphs.

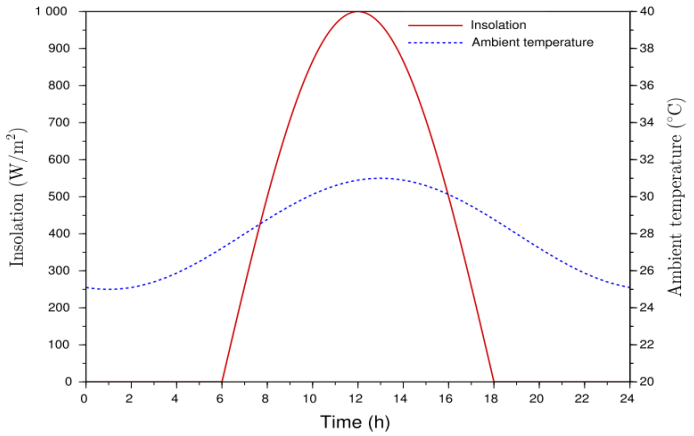

***Figure 3**: A graphical representation of the daily solar insolation and daily ambient temperature.*

3.2.1 Temperature profiles of first and second air flows

Fig. 4 is the graph of the temperature profiles of the first and second air flows. These profiles were determined using equations 2.27 and 2.28 respectively. The air flowing over the second absorber segment, T_{air2}, has a slightly higher peak temperature than the air that flows through the heat sink, T_{air1}. T_{air2} recorded a peak temperature of 318.5K, (45.5^{o}C) while T_{air1} got to a peak of 314.1K, (41.1^{o}C). T_{air1} initially enters the heat sink at ambient temperature, 298K, (25^{o}C), but it then picks up some heat dissipated at the heat sink of the TEGs and flows over the second absorber segment through a rectangular slit. While flowing over the second absorber, it becomes T_{air2} (where it gets heated further), as it flows over the very hot second absorber segment.

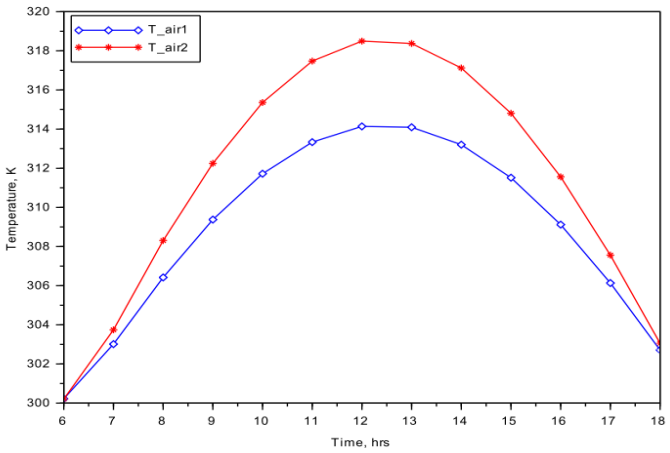

Figure 4: Hourly temperatures of the first and second air flows through the system, T_{air1} and T_{air2}.

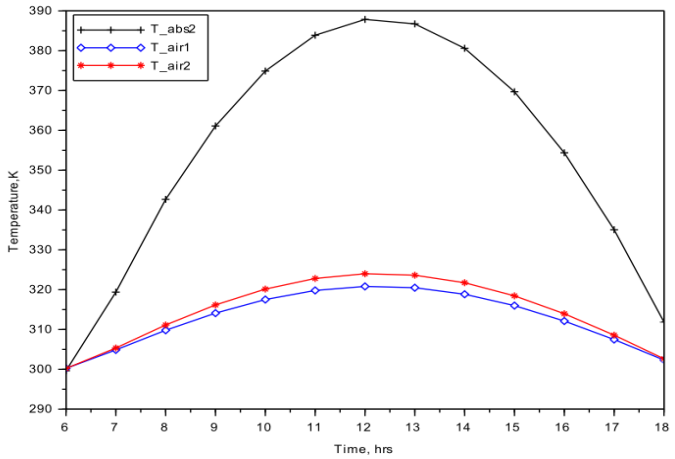

Figure 5: Hourly temperatures of the first and second air flows through the system and the temperatures of the second absorber temperature, T_{abs2}.

Fig. 5 is the graph showing the profile of the first and second air flows together with the second absorber segment respectively. The second absorber segment makes some contributions to the increase in energy of the first air mass which has just entered the space above it as the air flow moves to the exit. Although there was an increase in the energy content of the second air mass from what it used to be (first air mass) due to the heat from the second absorber segment, yet the increment does not seem to be proportionally high. It would be expected that the profile of the second air mass has its peak at least midway between the peak temperatures of T_{air1} and T_{abs2}.

A possible explanation for this anomalous situation could be due to the low thermal conductivity of air, 0.0271W/mK. This low value means that for every 1K rise in temperature through a length of 1m for a cross sectional area of $1m^2$, the heat transfer rate to the air is just 0.0271 Watts.

3.2.2 Temperature profiles of first and second absorber segments

Fig. 6 is a graph showing the temperature profiles for the first and second absorber segments. These profiles were determined using equations 2.29 and 2.30 respectively. The temperature profile of the second absorber segment reached a higher peak than that of the first absorber segment. The peak temperature of the second absorber segment was 397.4K, (124.4^{o}C) while that of the first was at 393.9K, (120.9^{o}C). The reason behind the disparity between the temperatures of the two absorber segments can be traced to the design of the Solar Collector-TEG system.

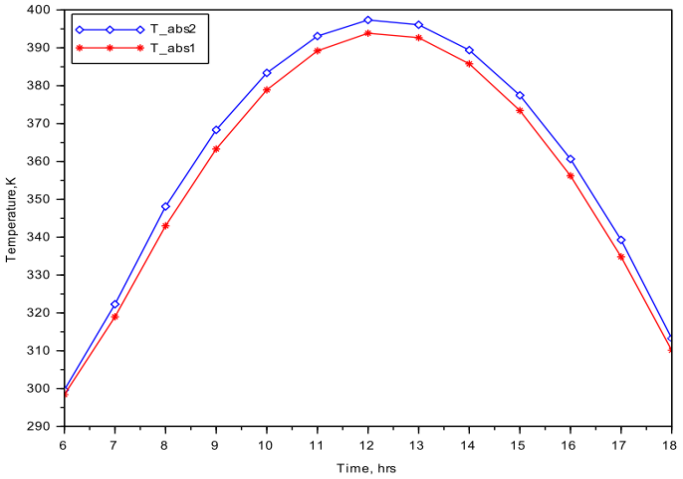

Figure 6: Hourly temperatures of the first, T_{abs1}, and second, T_{abs2}, absorber segments.

Whereas the TEGs were coupled to the first absorber (the heat source for the TEGs), there were no TEG couplings to the second absorber. Instead, the second absorber was properly insulated to reduce heat loss beneath the surface of the absorber. The first absorber segment with the TEGs coupled underneath it, loses heat by resistive heating and conduction through the thermoelements of the TEGs to the heat sink. This loss of heat to the heat sink by the first absorber most likely led to the lower peak in the temperature profile of the first absorber segment.

3.2.3 Temperature profiles of the heat sink and heat source

Fig. 7 is a graph that shows the temperature profiles of the heat source (first absorber segment) and heat sink. According to equations 2.29 and 2.31, the temperature profile of the heat source has a much higher peak temperature at 393.9K, (120.9^{o}C) compared to the heat sink, with its peak at 314.5K, (41.5^{o}C). The heat sink temperature of 120.9^{o}C is close to 140^{o}C which Rowe [19] presented as suitable for the operation of TEGs. Although heat is lost by resistive heating and conduction through the thermoelements, from the heat source to the heat sink, yet the heat source holds a much higher temperature profile. This is because the heat source is continuously heated by the sun's radiation whereas the heat sink is continuously being cooled by the inlet air (at ambient temperature) that flows into the space adjacent to the heat sink.

As a result of buoyancy, already heated air around the heat sink flows through the slit into the space above the second absorber segment, giving room for ambient air to continuously flow in to keep cooling the heat sink

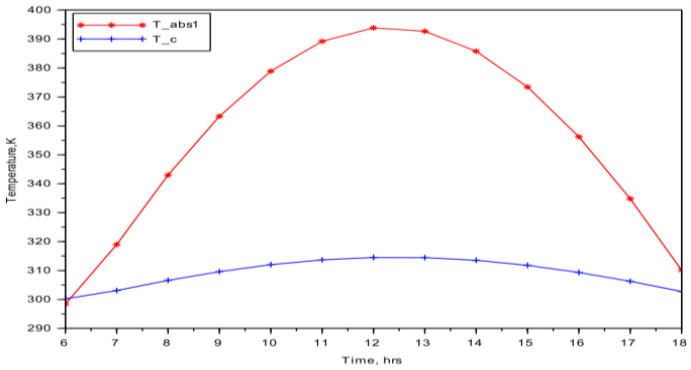

Figure 7: Hourly temperatures of the heat source, T_{abs1}, and heat sink, T_c.

3.3 TEG temperature difference between the heat sink and heat source against time

The temperature difference between the heat sink and the heat source increases with time during the first half of the day and gets to a peak value of 79.4º around midday in Fig. 8. It then falls in the second half of the day. The profile starts from a temperature difference that is below

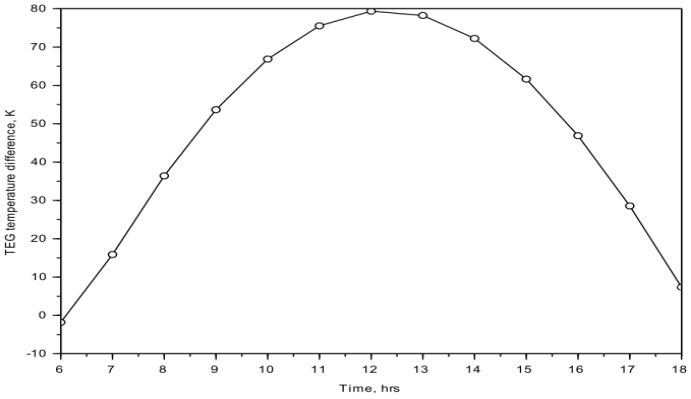

Figure 8: Temperature profile of the TEG temperature difference between heat source and heat sink

0 K. To understand this behavior, it should be pointed out that each simulation for the program is meant to run for a time step that represents one day (24 hours). During most of the daylight hours, the first absorber segment (the TEG heat source) is hotter than the heat sink. As evening approaches, the TEG heat source does not receive radiation any longer since the sun has gone down.

However, it continuously loses heat by conduction to the heat sink because it has a lower specific heat capacity (480J/kg.K) than the heat sink (900J/kg.K). At some point during the night, the heat sink then has a higher temperature than the heat source. This continues all through the rest of the night to the early hours of the morning, leading to negative TEG temperature difference. As soon as the sun's radiation starts coming up with increasing sunshine, the heat source then quickly becomes hotter than the heat sink and the TEG temperature difference becomes positive.

3.4 Output power, voltage and current characteristics of the TEGS

The profiles of the power and voltage generated from the TEGs are shown in Figs. 9a and 9b. The profiles were determined using equations 2.21 and 2.22respectively. Both the voltage and the power start rising from zero at the 6th hour of the day and get to a peak of 19.76 Volts and 12.56 Watts respectively around midday. However, by the 18th hour of the day, the power drops to almost zero while the voltage drops to 1.84 Volts. The reason why the power has a value of around 0 Watts even when the voltage was still somewhat substantial could be due to the value of the current in the 18th hour, (0.059 amperes). The profile for the current is shown in Fig. 10 and is determined using equation 2.18c. Since power is a product of current and voltage, then multiplying a very low current by a voltage of 1.84 volts would bring about a power value of almost 0 Watts.

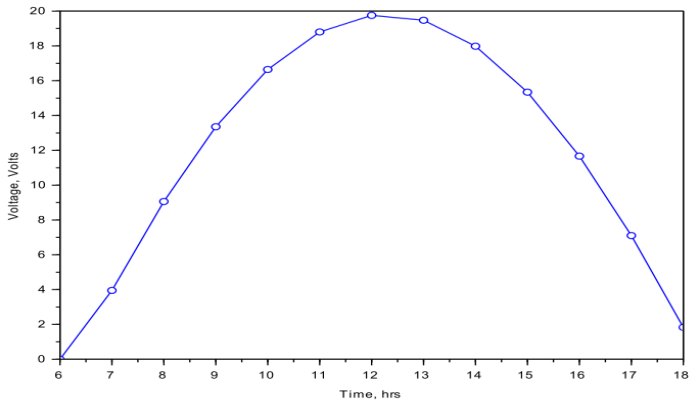

Figure 9a: A graphical representation of the voltage of the TEGs.

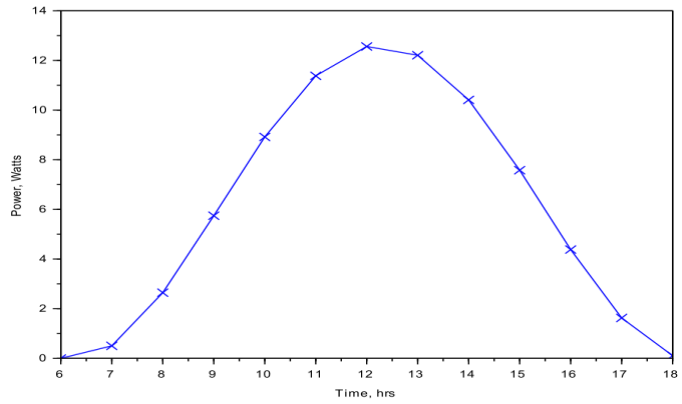

Figure 9b: A graphical representation of the power of the TEGs.

The maximum current shown in Fig. 10 is obtained around midday, and it has a value of 0.64 Amperes. This is 56% of the default design TEG current generation which is at 1.14 Amperes.

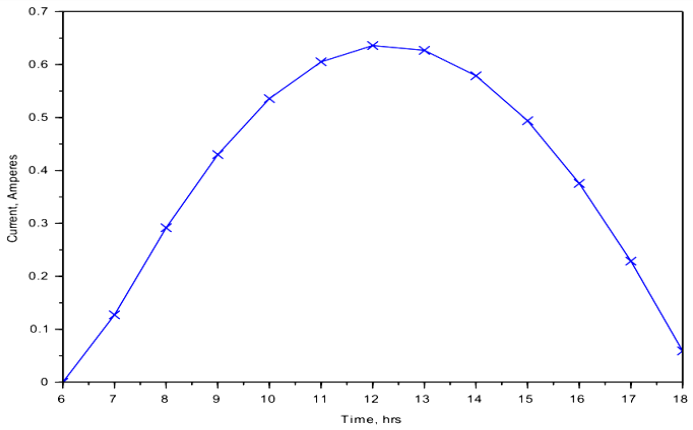

Figure 10: A graphical representation of the current generated from the TEGs.

3.5 Electrical efficiency of the TEGS

The graph showing the profile of the cumulative electrical efficiency of the TEGs is presented in Fig. 11. It is determined using equation 2.23a. There is a gradual increase from zero to a peak of 8.3% at around 3pm. Then from this hour, decline in the efficiency slowly sets in but not going lower than the 8% mark. The electrical efficiency of the TEGs obtained from this modeling is consistent with the value of 8% obtained in Biswas et al [18]. The decline noticed in the profile is in line with what was expected because insolation gradually decreases as evening sets in. Another reason could be due to increase in electrical resistance at the heat source (first absorber segment) as temperature of the first absorber segment rises. Furthermore, it can be observed that the electrical efficiency stayed around the 8% up to the 18th hour and this may have been because the first absorber segment of the collector was still hot around this time. The heat source temperatures between the hours of 3pm and 6pm ranged between 373.4K, (100.4^{o}C) and 310.1K, (37.1^{o}C) respectively while for the heat sink, the temperature ranged between 311.8K, (38.8^{o}C) and 302.7K, (29^{o}C) respectively. These temperature ranges are substantial values and adequate for the TEGs to function effectively.

3.6 Cumulative energy gained by the second absorber segment and energy gained by the air flowing to the exit.

The heat generated in the heated air and the energy gained by the second absorber segment are computed using equations 2.24b and 2.24a. Fig. 12 shows the profiles of the cumulative energy gained by the second absorber segment and that gained by the exit air for the daytime operation.

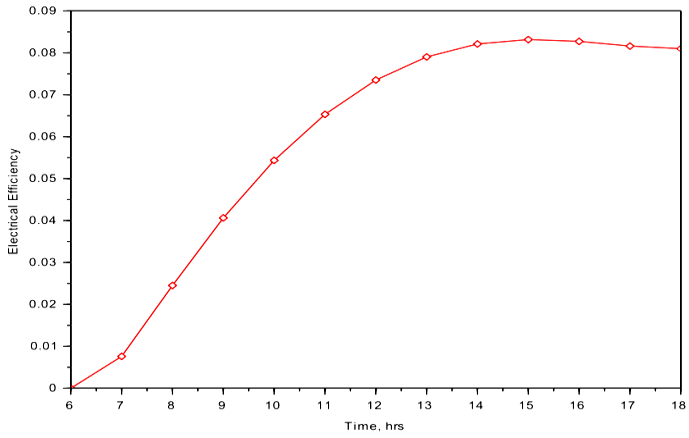

Figure 11: Daytime Electrical Efficiency of the TEGs.

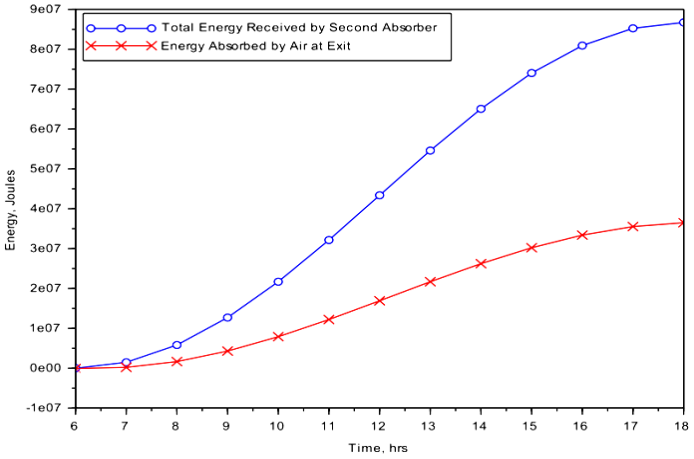

Figure 12: Cumulative energy absorbed by the second absorber segment of the solar collector and cumulative energy gained by the exit air.

It is important to assess the energy generated by the second absorber segment and in the exit air. It can be observed that both profiles start from zero but end up with much different peaks. Whereas the energy received in the second absorber rises to a cumulative peak value of 87 MJ, the peak of the exit air profile gets to 37 MJ. Some reasons could be responsible for this. Air has a lower specific heat capacity than the second absorber, thus heat gain by the two materials would not be the same. Another factor would be the mobility of the air. The air above the second absorber is not stagnant but in motion. Hence there might not be enough time for the air flowing to the exit to gain as much heat from the second absorber as would have been desired. Also, the second absorber segment does not transfer all energy it absorbs to the air. Some of the energy

is lost to the ambient via conduction through the insulator and via radiation through the glazing.

4.0 THERMAL EFFICIENCY OF THE SOLAR AIR HEATER

The thermal efficiency of the solar collector was determined using equation 2.24c and is shown in Fig. 14 for the daytime operation of the collector. A comparison of the energy gains shown in Fig. 13 will suggest that the collector's thermal efficiency will not exceed 50% since the exit air energy gain is not up to half of the gain by the second absorber segment. Fig. 14 shows that the profile of the thermal efficiency rises in a linear manner between 6am and 8am and thereafter assumes the shape of a curve. The profile gets to a peak thermal efficiency of 42%. This is consistent with the thermal efficiency recorded in Eze and Ojike in [14].

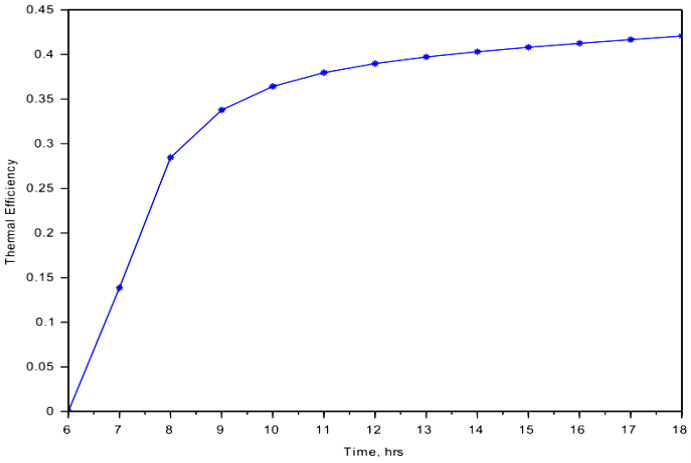

Figure 14: Day time thermal efficiency profile of the solar collector.

5.0 CONCLUSIONS

This work has presented a finite forward difference analysis of the transient behavior of a conjugate flat plate air heater-TEG collector, for heat and electricity generation. Mass and energy balances were carried out to determine the performance of the heat and electricity generation components of the collector. The maximum temperatures attained by the first air flow, 41.1^{o}C, the heat sink, 41.5^{o}C and the second air flow, 45.5^{o}C, were the lowest of all temperatures of components that were obtained in the control model designed for the work. The first glass segment and the second glass segment attained peak temperatures of 63.3^{o}C and 45.9^{o}C respectively. The first absorber (heat source) segment and the second absorber segment attained the highest temperatures of 120.9^{o}C and 124.4^{o}C. The electrical efficiency of the model was 8.3%, an increase of 0.3% from the work of Biswas et al [18]. The thermal efficiency of the collector of the model was 42% and is consistent with the value presented in Eze and Ojike in [14]. However there is some important point to make concerning the thermal efficiency of this system. In this research work, air was used as the fluid for heat transfer while in [8], water, which has a higher thermal conductivity than air, was used. It is expected that the efficiency of an air heating collector should be lower than that of a water heating collector. Thus, for this work (which is of a hybrid nature, since it comprises a TEG system in addition to the air heating collector) to have comparable efficiency, it is shows that a system designed by coupling a Flat Plate Air Heater Collector with Thermoelectric Generators, TEGs, is feasible and has good prospects.

6.0 FUNDING

This research work was carried out with the help of the financial resources provided by a scholarship received by one of the authors. The author, Abraham Chinedu Kalu-Uka is a recipient of the 2016 Petroleum Technology Development Fund PTDF LSS Scholarship for a master's degree programme in Energy and Power Technology.

REERENCES

[1] Bhusan B. Singh R. "A Review on Methodology of Artificial Roughness Used in Duct of Solar Air Heaters. Energy 2010;35:2012-2024.

[2] Suman S., Khan M.K., Pathak M. "Performance Enhancement of Solar Collectors-A Review". Renewable and Sustainable Energy Reviews. 2015(49):192-210.

[3] Towler G.P., Oroskar A.R., Smith S.E. "Development of a Sustainable Liquid Fuel Infrastructure Based on Biomass". Environmental Progress 2004;23(4):334-41.

[4] Thirugnanasambandam M., Iniyan S., Goric R. "A Review of Solar Thermal Technologies". Renewable and Sustainable Energy Reviews 2010;13:312-22.

[5] Ahmadi M.H., Ghazvini M., Sadeghzadeh M., Nazari M.A., Kumar R., Naeimi A., Ming T. "Solar Power Technology for Electricity Generation: A Critical Review". Energy Science and Engineering 2018;6(5):340-361.

[6] Mgbemene C, Duffy J.J, Sun H, Onyegegbu S. "Electricity Generation from a Compound Parabolic Concentrated Coupled to a Thermoelectric Module". Journal of Solar Energy 2010;132(3):31015(1-8).

[7] Amatya R, Ram R.J. "Solar Thermoelectric Generator for Micropower Applications". Journal of Electronic Materials 2010;39:1735-1740.

[8] Duffie J.A, Beckman W.A. "Solar Engineering of Thermal Processes". 3rd Edition. John Wiley and Sons. Inc. New York. 1991:150-165.
[9] Togrul I.T., Pehlivan D. The Performance of a Solar Air Heater with Conical Concentrator under Forced Convection. Int. Journal of Thermal Science 2003;42:571-652.
[10] Snyder G.J. "Small Thermoelectric Generators". The Electrochemical Society Interface; Fall 2008:54.
[11] Neville R.C. "Solar Energy Conversion, The Solar Cell". New York: Elsevier Scientific Publishing Company 1978:27-28.
[12] Enibe S.O. "Thermal Analysis of a Natural Circulation Solar Air Heater with Phase Change Materials Energy Storage". Journal of Renewable Energy 2003;28(14):2269-2299.
[13] Saxena A., Varun, El-Sebaii A. A. "A Thermodynamic Review of Solar Air Heaters". Renewable and Sustainable Energy Reviews 2015;43:863-890.
[14] Eze J.I, Ojike O. "Analysis of Thermal Efficiency of a Passive Solar Water Heater". International Journal of Physical Sciences. 2012:7(22):2891-2896.
[15] Indragit, Bansal N.K., Garg H.P. "An Experimental Study on a Finned Type and Non Porous Type Solar Air Heater with a Solar Simulator". Energy conversion and Management 1985;25(2):135-143.
[16] Singh D., Bansal N.K. "Analysis of a Glass Solar Air Heater". Energy Conversion and Management 1983;23(4):231-237.
[17] Bjork R, Christensen D.V, Eriksen D, Pryds N. "Analysis of the Internal Heat losses in a Thermoelectric Generator". International Journal of Thermal Sciences 2014;85:12-20.
[18] Biswas K, Jiaqing H, Blum I.D, Wu C, Hogan T.P, Seidman D.N, Dravid V.P, Kanatzidis M.G. "Analysis of the Internal Heat losses in a Thermoelectric Generator". International Journal of Thermal Sciences, 2012:489:414-418.
[19] Rowe D.M. "Thermoelectrics, an Environmentally-Friendly Source of Electrical Power. Renewable Energy 1999;16:1251-1256.
[20] Rajput R.K. "Heat and Mass Transfer". Schand Publishing Company, New Delhi, India. 2012:373-538,753.
[21] Padilla V.P., Demirkaya G., Goswami D.Y., Stefanakos E., Rahman M.M. "Heat Transfer analysis of Parabolic Trough Solar Receiver". Applied Energy. 2011:88:5097-5110.
[22] Iloeje O.C. "Introductory Course in Heat and Mass Transfer". University of Nigeria, Press Ltd. Nsukka, Nigeria. 2018;135-145.
[23] Cengel Y.A., Ghajar A.J. "Heat and Mass Transfer, Fundamentals and Applications". 5th Edition. Mc Graw Hill Education. New York. 2006:511.
[24] Angrist S.W., "Direct Energy Conversion, Boston, MA, Allyn and Bacon Inc. ISBN 0205077587.
[25] Torchia-Nunez J.C., Porta-Gandara M.A., Cervantes J. "Exergy Analysis of a Passive Solar Still". Renewable Energy. 2008:33(4):606-616.

APPENDIX

Table 2.1: The parameters of the glass

Length of first glass segment	0.4m
Width of first glass segment	0.4m
Length of second glass segment	0.7m
Width of second glass segment	0.4m
Absorptivity of the glass	0.14
Transmitivity of the glass	0.83
Emissivity of the glass	0.95
Density of the glass	2800kg/m^3
Specific heat capacity of the glass	800J/kg.K

Table 2.2: The parameters of the absorber segment

Length of first absorber segment	0.4m
Width of first absorber segment	0.4m
Length of second absorber segment	0.6m
Width of second absorber segment	0.4m
Thickness of absorber	0.002m
Gap spacing between glazing and absorber	0.025m
Absorptivity of the absorber plate	0.95
Emissivity of the absorber plate	0.90

Density of absorber	8800kg/m^3
Thermal conductivity of absorber	0.733W/m.K
Specific heat capacity of absorber	480J/kg.K
Length of first absorber segment	0.4m
Width of first absorber segment	0.4m
Length of second absorber segment	0.6m
Width of second absorber segment	0.4m
Thickness of absorber	0.002m
Gap spacing between glazing and absorber	0.025m
Absorptivity of the absorber plate	0.95
Emissivity of the absorber plate	0.90
Density of absorber	8800kg/m^3
Thermal conductivity of absorber	0.733W/m.K
Specific heat capacity of absorber	480J/kg.K

Table 2.3: Properties of air

Density of air	1.27kg/m^3
Kinematic viscosity of air	$15.89^{x}10^{-6}$m^2/s
Thermal conductivity of air	0.0271W/mK
Specific heat capacity of air	1003J/kgK
Wind velocity over the collector surface	3m/s
Air velocity through the collector	2m/s

Table 2.4: Parameters of the Thermoelectric Module TEM

Seebeck coefficient	$3.92^{x}10^{-4}$V/C
Resistivity of each TEM	$1.4^{x}10^{-5}$Ωm
Thermal conductivity of each TEM	1.63W/mC
Surface dimension of each TEM	$0.04^{x}0.04$m^2
Number of Thermoelements per module	127
Area to length ratio of Thermoelements	0.00121
Number of Thermoelectric Generators	10

Table 2.5: Properties of the heat sink and fins

Length of each heat sink	0.135m
Width of each heat sink	0.105m
Base thickness of each heat sink	0.008m
Number of heat sinks	11.29
Width of heat sink space	0.4m
Length of heat sink space	0.4m
Gap spacing for the heat sink	0.04m
Density of heat sink	2700kg/m^3
Specific heat capacity of heat sink	900J/kg.K
Number of fins per heat sink	14
Total Number of fins	158
Length of each fin	0.135m
Width of fin	0.002m
Height of fin	0.025m
Thermal conductivity of fin	240W/m.K
Fin efficiency	0.90

Table 2.6: Properties of the insulation material

Thermal conductivity of insulation, Glass wool	0.045W/m.K
Length of first insulation segment	0.4m
Width of first insulation segment	0.4m
Length of second insulation segment	0.6m
Width of second insulation segment	0.4m

Table 2.7: Other parameters

Tilt angle of the collector	22^o
Acceleration due to gravity	$9.81m/s^2$
Surface heat transfer coefficient of fin	$27W/m^2.K$
Angle the connector of the heat sink base component makes with second absorber	60^o